Experimental Neurology 372 (2024) 114632

Contents lists available at ScienceDirect

Experimental Neurology

journal homepage: www.elsevier.com/locate/yexnr

Research paper

Fragmentation of functional resting state brain networks in a transgenic mouse model of tau pathology: A metabolic connectivity study using [^{18}F] FDG-PET

Heike Endepols [a,b,c], Marta Anglada-Huguet [d], Eckhard Mandelkow [d,e], Bernd Neumaier [a,b,*], Eva-Maria Mandelkow [d,e], Alexander Drzezga [c,d,f]

[a] University of Cologne, Faculty of Medicine and University Hospital Cologne, Institute of Radiochemistry and Experimental Molecular Imaging, Cologne, Germany
[b] Forschungszentrum Jülich GmbH, Institute of Neuroscience and Medicine, Nuclear Chemistry (INM-5), Wilhelm-Johnen-Straße, Jülich 52428, Germany
[c] University of Cologne, Faculty of Medicine and University Hospital Cologne, Department of Nuclear Medicine, Cologne, Germany
[d] German Center for Neurodegenerative Diseases (DZNE), Bonn-Cologne, Germany
[e] Department Neurodegenerative Diseases & Gerontopsychiatry, University Hospital Bonn, Germany
[f] Forschungszentrum Jülich GmbH, Institute of Neuroscience and Medicine, Molecular Organization of the Brain (INM-2), Wilhelm-Johnen-Straße, Jülich 52428, Germany

ARTICLE INFO

Keywords:
Small animal PET
Metabolic connectivity
Tauopathy mouse model

ABSTRACT

In a previous study, regional reductions in cerebral glucose metabolism have been demonstrated in the tauopathy mouse model rTg4510 (Endepols et al., 2022). Notably, glucose hypometabolism was present in some brain regions without co-localized synaptic degeneration measured with [^{18}F]UCB-H. We hypothesized that in those regions hypometabolism may reflect reduced functional connectivity rather than synaptic damage. To test this hypothesis, we performed seed-based metabolic connectivity analyses using [^{18}F]FDG-PET data in this mouse model. Eight rTg4510 mice at the age of seven months and 8 non-transgenic littermates were injected intraperitoneally with 11.1 ± 0.8 MBq [^{18}F]FDG and spent a 35-min uptake period awake in single cages. Subsequently, they were anesthetized and measured in a small animal PET scanner for 30 min. Three seed-based connectivity analyses were performed per group. Seeds were selected for apparent mismatch between [^{18}F]FDG and [^{18}F]UCB-H. A seed was placed either in the medial orbitofrontal cortex, dorsal hippocampus or dorsal thalamus, and correlated with all other voxels of the brain across animals. In the control group, the emerging correlative pattern was strongly overlapping for all three seed locations, indicating a uniform fronto-thalamo-hippocampal resting state network. In contrast, rTg4510 mice showed three distinct networks with minimal overlap. Frontal and thalamic networks were greatly diminished. The hippocampus, however, formed a new network with the whole parietal cortex. We conclude that resting-state functional networks are fragmented in the brain of rTg4510 mice. Thus, hypometabolism can be explained by reduced functional connectivity of brain areas devoid of tau-related pathology, such as the thalamus.

1. Introduction

Transgenic animal models have contributed immensely to the discovery of pathological mechanisms present in human neurodegenerative diseases. They allow focusing on the impact of specific factors, while other factors are controlled for or not present at all. One well-studied example is the rTg4510 mouse model which expresses human tau (isoform 0N4R) with the P301L mutation mostly in the hippocampus, cortex, olfactory bulb and striatum (Santacruz et al., 2005). We found previously in a multi-tracer PET study that those mice show tau deposition, neuroinflammation and synaptic degeneration in the regions of mutated tau expression. However, hypometabolism measured with the tracer [^{18}F]FDG was much more widespread, occuring in brain regions entirely devoid of tau-related pathology, such as the thalamus (Endepols et al., 2022). In particular, the mismatch between hypometabolism and synaptic degeneration was puzzling, as cerebral [^{18}F]FDG uptake is a

* Corresponding author at: Forschungszentrum Jülich GmbH, Institute of Neuroscience and Medicine, Nuclear Chemistry (INM-5), Leo-Brandt-Straße, Bldg. 15.19, Jülich 52425, Germany.
E-mail address: b.neumaier@fz-juelich.de (B. Neumaier).

https://doi.org/10.1016/j.expneurol.2023.114632
Received 24 August 2023; Received in revised form 7 November 2023; Accepted 29 November 2023
Available online 3 December 2023

surrogate marker for glucose consumption and reflects synaptic activity (Dienel et al., 2018; Raichle and Mintun, 2006; Schwartz et al., 1979). A strong correlation between brain glucose utilization and expression of synaptic vesicle proteins was therefore expected and has already been shown in previous studies (Rocher et al., 2003; van Aalst et al., 2021). However, during both healthy aging and neurodegenerative diseases, changes in synaptic density and glucose utilisazion are not correlated to the same extent in all brain areas (Andersen et al., 2022; Chen et al., 2021; Delva et al., 2022), suggesting that other factors contribute to glucose metabolism as well. Apart from synaptic atrophy, hypometabolism may also be caused by reduced activity of structurally intact synapses, reflecting reduced functional connectivity. It has indeed been shown in previous studies that functional connectivity and glucose metabolism are closely related (Drzezga et al., 2011; Kato et al., 2016; Marchitelli et al., 2018; Passow et al., 2015; Schmitz et al., 2021). Hypometabolism may therefore occur in a preserved structural network, which is nevertheless functionally compromised due to reduced input from tau-affected areas. To test this hypothesis, we performed seed-based metabolic connectivity analyses with the [^{18}F]FDG images of all animals included in our recent study (Endepols et al., 2022). This approach relies on the assumption that glucose consumption of functionally connected brain areas shows a mathematical correlation, and has proven a successful method to study functional brain networks in humans (Riedl et al., 2016; Yakushev et al., 2017). In previous studies we and others have shown that seed-based metabolic connectivity analysis is suitable for rodent models as well (Apetz et al., 2019; Huo et al., 2021; Rohleder et al., 2016). We hypothesized that metabolic connectivity would be reduced in rTg4510 mice compared to non-transgenic littermates.

2. Materials & methods

2.1. Study design

Two groups of mice (transgenic rTg4510 mice expressing human tau with the P301L mutation [$n = 8$] and non-transgenic littermates as controls [n = 8], seven months of age) were compared with respect to metabolic brain connectivity. Seed-based analysis based on [^{18}F]FDG PET-images was used with seeds placed in the medial orbital cortex (midline), left dorsal hippocampus, and left dorsal thalamus.

2.2. Animals

Experiments were carried out in accordance with the EU directive 2010/63/EU for animal experiments and the German Animal Welfare Act (TierSchG, 2006) and were approved by the regional authorities (LANUV NRW; application number 84–02.04.2015.A234 and 81–02.04.2018.A313). The ARRIVE guidelines 2.0 were followed.

The transgenic mouse model rTg4510 expresses the tau isoform 0N4R (Uniprot P-10636-D, alias “htau24”, 383 residues) with the FTDP17 mutation P301L (Ramsden et al., 2005; Santacruz et al., 2005). Briefly, rTg4510 animals were produced by crossing the activator mouse line CaMK2a-tTA (background C57BL/6), with the responder tetO. MAPT*P301L mouse line (background FVB). Mice having both the CaMK2a-tTA and tau transgene expressed human mutant P301L tau at high levels, up to ~13 times of murine tau. Mature tangles are present from 4 months of age (Santacruz et al., 2005). Mice lacking the responder and the activator transgene were used as controls. Mice were screened by PCR using the following primer pairs: hTau transgene (Tau mPrP_E2): forward 5′-TGA ACC ATT TCA ACC GAG CTG-3′; reverse: 5’-TAC GTC CCA GCG TGA TCT TC-3′; CaMK2 promoter (oIMR8746/oIMR8747): forward 5’-CGC TGT GGG GCA TTT TAC TTT AG-3′; reverse: 5’-CAT GTC CAG ATC GAA ATC GTC-3′.

Sixteen adult mice were used for this study: eight rTg4510 mice (five females, three males; 22–29 g body weight) and eight non-transgenic littermates (four females, four males; 39–54 g body weight) at the age of seven months. All measured animals were included in the analysis. The mice were housed in groups in individually ventilated cages (NextGen, Ecoflow, Phantom, Allentown) under controlled ambient conditions (22 ± 1 °C and 55 ± 5% relative humidity) with a 12-h light/dark schedule and ad libitum access to food and water. Cages were enriched with nestlets, chew blocks and shelters.

2.3. Positron Emission Tomography (PET)

From our earlier study (Endepols et al., 2022), we used PET data produced with the SV2A tracer [^{18}F]UCB-H ($n = 5$ per group) and the glucose tracer [^{18}F]FDG ($n = 8$ per group) to analyze correlation between the two tracers, and for metabolic connectivity analysis with [^{18}F]FDG.

[^{18}F]UCB-H was synthesized on a Trasis All-In-One synthesizer according to Warnier et al. (Warnier et al., 2016). Animals were anesthetized with isoflurane in O_2/air 3:7 (induction 5%, maintenance 1.5–2.0%), and a catheter for tracer injection was inserted into the lateral tail vein. Mice were placed on an animal holder (medres® GmbH, Cologne, Germany) and fixed with a tooth bar in a respiratory mask. Body temperature was maintained at 37 °C using a feedback-controlled warming system. Eyes were protected from drying out by application of eye and nose ointment (Bepanthen, Bayer). A PET scan in list mode was conducted using a Focus 220 micro PET scanner (CTI-Siemens, Erlangen, Germany) with a resolution at the center of field of view of 1.4 mm. Data acquisition started with intravenous [^{18}F]UCB-H injection (10.1 ± 0.5 MBq in 125 μl) and lasted for 60 min. This was followed by a 10 min transmission scan using a ^{57}Co point source for attenuation correction. After the scan was finished, the catheter was removed and the mice were returned to their home cage.

[^{18}F]FDG was purchased from Life Radiopharma Bonn GmbH. Animals were anesthetized with isoflurane in O_2/air 3:7 (induction 5%, maintenance 1.5–2.0%) for 2–5 min, and 11.1 ± 0.8 MBq [^{18}F]FDG in 125 μl were injected intraperitoneally. The mice were then placed in a solitary cage without food, where they spent the following 35 min awake. Subsequently, they were anesthetized again and placed on the animal holder. The scan started 40 min after [^{18}F]FDG injection and had a duration of 30 min. This was followed by a transmission scan (see above). This protocol takes advantage of metabolic trapping of [^{18}F]FDG (Pauwels et al., 1998), which allows awake tracer uptake and subsequent scanning under anesthesia (Cui et al., 2020; Kordys et al., 2017). Blinding was used for PET measurements.

2.4. Image reconstruction and postprocessing

After full 3D rebinning, summed images were reconstructed using an iterative OSEM3D/MAP procedure (Qi et al., 1998), resulting in voxel sizes of 0.47 × 0.47 × 0.80 mm. For all further processing of the images including statistics, the software VINCI 4.72 for MacOS X (Max Planck Institute for Metabolism Research, Cologne, Germany) was used. Images were co-registered and intensity-normalized to cerebellum, where the tau transgene is not expressed. Each image was divided by the mean value of the cerebellum VOI (elliptical, 4 mm^3), resulting in the “background-standardized uptake value ratio” ($SUVR_{Cer}$). For seed-based connectivity analysis, the images were Gauss-filtered with 1 mm FWHM.

2.5. Metabolic connectivity analysis

No blinding was used for connectivity analysis, as we already knew group assignments from the previous analysis. We selected three seeds based on results from our previous analysis (Endepols et al., 2022), which are shown here projected on the sections containing the seeds (Fig. 1). As a first step, we looked at the voxel-wise difference maps resulting from statistical comparison (t-test) between rTg4510 mice and non-transgenic littermates (=controls) for the tracers [^{18}F]FDG and [^{18}F]UCB-H. Although both directions (“rTg4510 < controls” and

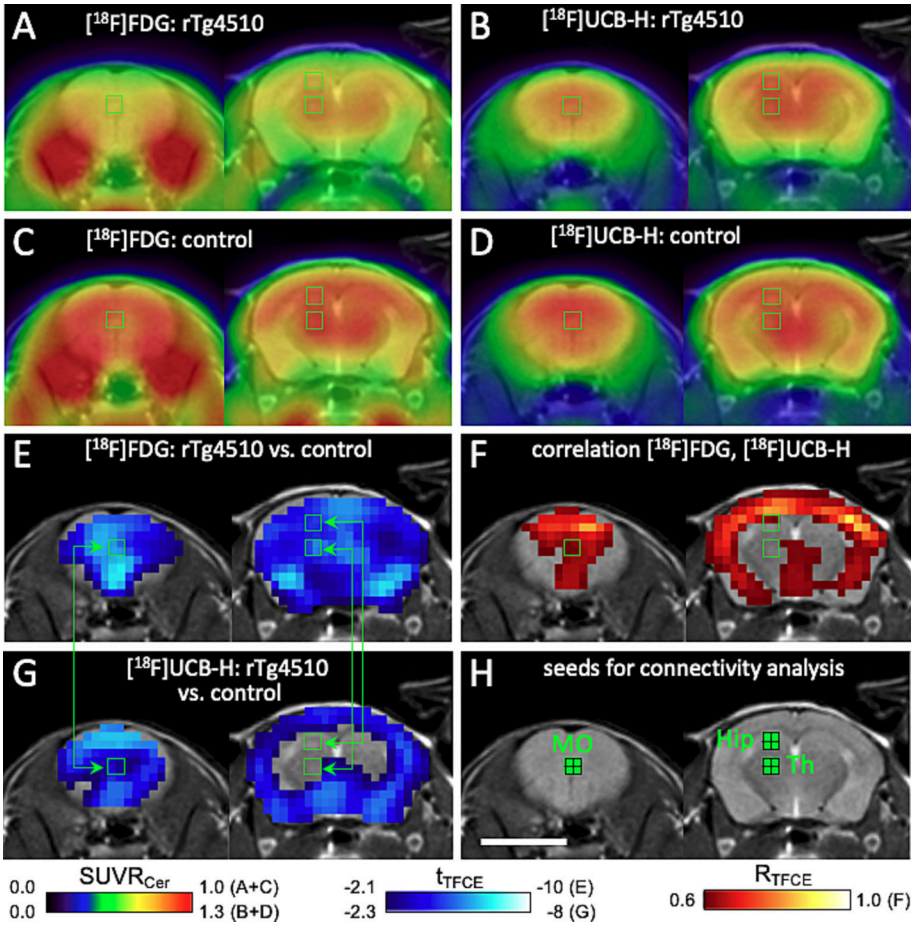

Fig. 1. Seed selection based on mismatch between hypometabolism and reduction of synaptic density. In each subfigure, the same two transverse section levels are displayed: +2.8 mm and − 1.8 mm from Bregma. The data from A–G has already been shown in (Endepols et al., 2022) for other section levels. (A + C) [^{18}F]FDG mean images; (B + D): [^{18}F]UCB-H mean images; (E + G): Difference maps for [^{18}F]FDG and [^{18}F]UCB-H, respectively, projected onto an MRI template. Blue voxels indicate significantly lower tracer uptake in rTg4510 mice ("rTg4510 < controls"). Seeds (green outlines) were placed in locations where hypometabolism was present (A + E), but no or little synaptic degeneration (B + G). Green arrows indicate the respective comparisons. (F): Mismatch between [^{18}F]FDG and [^{18}F]UCB-H is further demonstrated by low or absent positive correlation between tracers. Red voxels indicate significant positive correlations, negative correlations were not present. (H): Location of the seeds (green), consisting of four voxels each. Scale bar: 5 mm. Abbreviations: Hip - hippocampus; MO - medial orbital cortex; Th - thalamus. (For interpretation of the references to colour in this figure legend, the reader is referred to the web version of this article.)

"controls < rTg4510") were tested, significant results were only achieved for "rTg4510 < controls ". A mismatch between [^{18}F]FDG (Fig. 1E) and [^{18}F]UCB-H (Fig. 1G) difference maps was present in the hippocampus and the thalamus, and also in the orbitofrontal cortex, although less striking. As a second step, we used the results of a Pearson correlation analysis between [^{18}F]FDG and [^{18}F]UCB-H (Fig. 1F). As expected, there was a positive correlation between tracers in many brain areas, while negative correlations did not occur. Notably, we found little or no positive correlation in the areas which already stood out in the comparison of the [^{18}F]FDG and [^{18}F]UCB-H difference maps. Based on these observations, three seeds of 4 voxels each (total volume of 0.72 mm^3) were placed in the medial orbital cortex (MO; part of the ventromedial prefrontal cortex), left dorsal hippocampus, and left dorsal thalamus (Fig. 1G). The thalamus seed covered the mediorostral part of the lateral posterior thalamic nucleus, and the dorsal part of the subjacent posterior thalamic nuclear group.

Mean seed values were extracted from every mouse, and a Pearson correlation analysis of the seed with all other voxels of the brain was performed across all animals of one group (rTg4510 or control, $n = 8$ each) for every seed. The resulting correlation maps were corrected for multiple testing using a threshold-free cluster enhancement (TFCE) procedure with subsequent permutation testing, thresholded at $p < 0.05$ (Smith and Nichols, 2009). TFCE and final thresholding was performed in VINCI using a python script. Permutation testing was done in RStudio 1.0 for Mac OS X. This yielded six connectivity maps (3 seeds × 2 groups) with brain voxels positively (displayed in red) or negatively (displayed in blue) correlated to the seed region. Positive correlations of brain voxels indicate that [^{18}F]FDG uptake was similar to the seed: In animals where seed uptake was high, red-labeled voxels also had high uptake. Similar to positive correlations in fMRI functional connectivity analysis, positive correlations in metabolic connectivity represent functional connections between brain areas (Friston, 2011; Yakushev et al., 2017). Negative correlations indicated an [^{18}F]FDG uptake inverse to the seed: In animals where the seed had high uptake, uptake of blue-labeled voxels was low, and vice versa. Negative correlations are thought to reflect regulatory interactions between brain regions, such as reciprocal modulations, suppression, inhibition and neurofeedback (Gopinath et al., 2015).

3. Results

Seed-based metabolic connectivity analyses were conducted with resting state [^{18}F]FDG images of rTg4510 mice ($n = 8$) and age-matched non-transgenic littermates (n = 8). Three seeds were used: medial orbitofrontal cortex (MO), left dorsal hippocampus, and left dorsal thalamus. The results of the wildtype control group are shown in Fig. 2A.

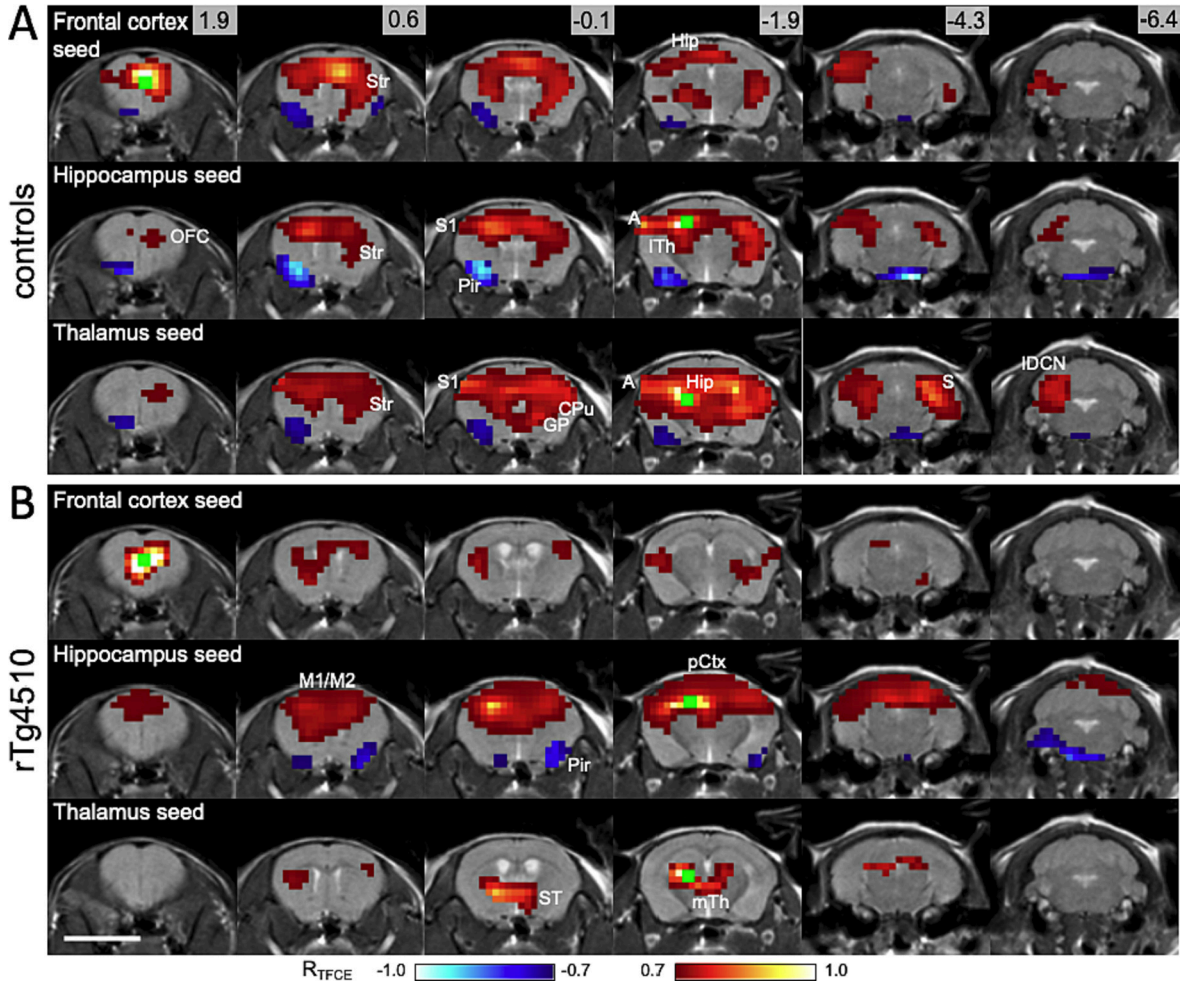

Fig. 2. Seed-based metabolic connectivity analysis. Shown are the statistical results (corrected for multiple testing) of Pearson correlation analysis of the seed region and the rest of the brain, projected onto an MRI template. (A) Control group ($n = 8$). (B) rTg4510 group (n = 8). Each row represents the metabolic connections of one seed (green). Positive correlations are depicted in red, negative correlations in blue. Numbers in the top row indicate rostro-caudal coordinates, i.e. distance from Bregma in mm. Scale bar: 5 mm. (For interpretation of the references to colour in this figure legend, the reader is referred to the web version of this article.)
Abbreviations: A - auditory cortex, CPu - caudate-putamen, GP - globus pallidus, Hip - hippocampus, lDCN - lateral deep cerebellar nuclei, lTh - lateral thalamus, mTh - medial thalamus, OFC - orbitofrontal cortex, pCtx - parietal cortex, Pir - piriform cortex, S1 - somatosensory cortex, ST - stria terminalis, Str - striatum.

The emerging correlation patterns looked highly similar for the three seeds: Positive correlations comprised somatosensory and motor cortex, anterior cingulate cortex, retrosplenial cortex, visual cortex, temporal association cortex, auditory cortex, striatum, subiculum, and lateral parts of the cerebellum. Negative correlations appeared in the left piriform cortex. The similarity of the connectivity patterns suggests that the three seeds were part of the same functional network. In contrast, for the rTg4510 group the analysis using the three seeds revealed distinctly different connectivity patterns; there was hardly any spatial overlap between the three correlation maps within the group of rTg4510 animals. [^{18}F]FDG uptake of the MO seed was correlated with parts of the striatum and auditory cortex. The dorsal thalamus seed was correlated with the stria terminalis region and the contralateral thalamus. While the frontal and thalamic networks were drastically diminished compared to controls, the hippocampus network had increased, now covering the entire parietal cortex and the dorsal striatum. Negative correlation between the hippocampus seed and the piriform cortex remained the same as in the control group. For network quantification see Table 1. Results from seeds in the right dorsal hippocampus and right dorsal thalamus were similar (supplemental Fig. 1).

Table 1
Comparison of seed-associated networks. Only positive correlations were used for quantification.

	controls			rTg4510		
seed	MO	dTh	Hip	MO	dTh	Hip
connected volume	133 mm^3	201 mm^3	115 mm^3	55 mm^3	28 mm^3	166 mm^3
mean R	0.85	0.85	0.89	0.80	0.79	0.84
network overlap		82.3 mm^3			0.7 mm^3	

Abbreviations: Hip - hippocampus; MO - medial orbitofrontal cortex; R - correlation coefficient; dTh - dorsal thalamus.

4. Discussion

In this work, we have chosen three seeds according to the greatest mismatch between [^{18}F]FDG-PET (glucose metabolism) and [^{18}F]UCB-H-PET (SV2A density) in rTg4510 mice (Endepols et al., 2022): MO (frontal cortex), hippocampus and dorsal thalamus. Our hypothesis was that the mismatch may be explained by reduced functional connectivity of these brain regions, which may lead to lower glucose consumption while synaptic integrity is still mostly intact. To test this hypothesis, we

performed a functional connectivity analysis on the basis of FDG-PET data obtained in transgenic and wildtype animals.

The main result was that in non-transgenic control mice the three selected seeds were components of the same network (Fig. 3A). Since tracer uptake took place while the mice were in single cages without any behavioral task, we expected resting state networks to originate from the frontal cortex seed. Indeed, most emerging regions were part of the default mode network (DMN) previously described for mice in fMRI studies (Ben-Nejma et al., 2019; Coletta et al., 2020; Liska et al., 2015; Stafford et al., 2014; Whitesell et al., 2021): frontal cortex, cingulate cortex, retrosplenial cortex, visual cortex, temporal association cortex, and striatum. While hippocampus and dorsal thalamus are often thought to form their own resting-state networks separate from the DMN (Grandjean et al., 2020; Liska et al., 2015), other researchers attributed the dorsal thalamus (Coletta et al., 2020; Whitesell et al., 2021) and the hippocampus (Ben-Nejma et al., 2019) to the DMN, which is supported by our results. The piriform cortex, which was negatively correlated to the seed regions in our study, has been considered to be part of the DMN as well (Ji et al., 2018). However, it should be noted that the piriform cortex receives some spill-over from the lateral pterygoid muscles (see supplemental Fig. 2), which might indicate a negative correlation between hippocampal activity and pterygoid muscle tone rather than involvement of the piriform cortex in the hippocampal network. The inconsistency in the literature with regard to the exact DMN components might result from different degrees of sedation in the abovementioned fMRI studies, which may decrease functional connectivity (Wang et al., 2021). In our metabolic connectivity study, the mice were fully awake during tracer uptake, which may explain the strong correlation between DMN core regions, piriform cortex, hippocampus and dorsal thalamus, forming one large resting-state network.

In rTg4510 mice, however, the connectivity analysis based on the identical three seeds revealed three functional networks, which were completely separate from each other (Fig. 3B). Compared to the networks in wildtype animals, the frontal cortex and dorsal thalamus networks showed particularly diminished extension in rTg4510 mice. Reduced frontal and/or thalamic connectivity has also previously been described in other studies on AD mouse models (Ben-Nejma et al., 2019; Bero et al., 2012; Green et al., 2019; Shah et al., 2013). Because the thalamus did not show any reduction of synaptic density (Endepols et al., 2022), it appears particularly likely that the observed thalamic hypometabolism can be explained by the reduced functional connectivity as demonstrated in the current study. In the frontal cortex, slightly reduced synaptic density (see Fig. 1B) may have contributed to some extent to hypometabolism in addition to decreased network activity.

Surprisingly, the hippocampal seed yielded a large network covering the whole parietal cortex and the dorsal part of the striatum in rTg4510 mice. Previous studies have shown that hippocampus and parietal cortex can form a shared functional network during resting state (Hall et al., 2022; Karatas et al., 2021), but usually these circuits are restricted to certain parietal areas and are involved in numerous functional aspects (Zheng et al., 2021). The situation where almost the whole cortex is functionally connected to the hippocampus has been previously described as hyperconnectivity in another tauopathy mouse model and interpreted as a compensatory phenomenon (Degiorgis et al., 2020). As the parietal cortex in rTg4510 mice suffers from considerable synaptic degeneration (Fig. 1G), hippocampal hyperconnectivity may nevertheless be consistent with hypometabolism.

In contrast to our findings, other studies reported reduced connectivity of the hippocampus in 3xTg-AD mice (with tau and amyloid β pathology) (Manno et al., 2019) and APPKI mice (amyloid β pathology) (Morrissey et al., 2022). However, it has recently been shown that the rTg4510 mouse displays other confounding factors, such as the *Fgf*14-TgINDEL mutation (Gamache et al., 2019; Goodwin et al., 2019): The intracellular fibroblast growth factor 14 (FGF14) binds to voltage-gated sodium channels at the axonal initial segment and is involved in regulation of neuronal excitability, synaptic plasticity and maturation of newly generated neurons (Di Re et al., 2017). Insertion of the *tetO-MAPT*P301L* transgene leads to a 244 kbp deletion in the *Fgf14* locus on chromosome 14, while approx. 70 transgene copies are integrated. This leaves the coding region of the splice variant V1 (encoding isoform 1a) intact, while the variants V2 (encoding isoform 1b), X1 and X2 are damaged (Gamache et al., 2019), resulting in altered current densities in the different subtypes of voltage-gated sodium channels (Laezza et al., 2009). It is therefore plausible that the observed changes in metabolic connectivity can not be attributed to tau pathology alone, but also to altered neuronal excitability caused by the *Fgf*14-TgINDEL mutation.

Taken together, our results demonstrate the fragmentation of one large uniform resting state network, as seen in the control animals, into three separate functional networks in rTg4510 mice. As a result of this fragmentation, thalamic and frontal cortex functional networks were strongly diminished in size. This finding could explain hypometabolism of those areas, as result of reduced neuronal input, in accordance with our initial hypothesis. The hippocampus also separated from the original network, but formed an even larger functional network with the parietal cortex. Hippocampal hypometabolism might be caused by impaired population activity in the hippocampal-parietal network.

4.1. Limitations

In contrast to fMRI, metabolic connectivity analysis is based on static PET images rather than time series. There is a debate about how well metabolic and functional connectivity results overlap, and which method gives the "true" results (Jamadar et al., 2021; Sala et al., 2022). The current understanding is that both methods produce valuable information about the communication between brain areas (Sala et al., 2023). One disadvantage of static metabolic connectivity analysis is that correlations are calculated across a group, and individual connectivity maps are not available. For this reason, our conclusions remain somewhat speculative and have to be further substantiated by individual results.

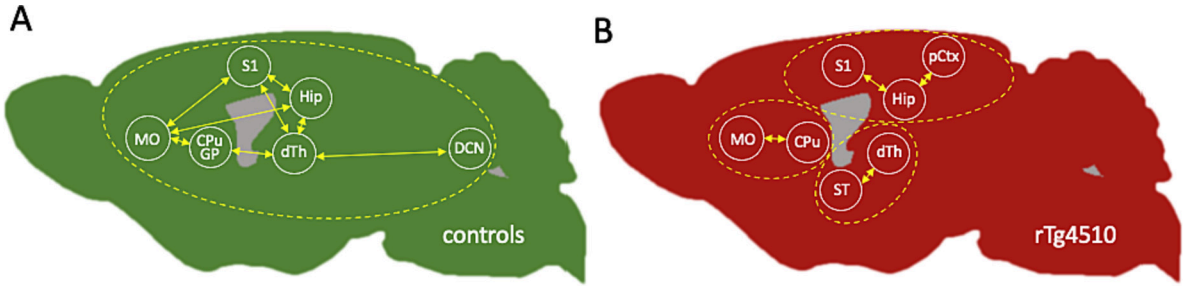

Fig. 3. Schematic drawing of metabolic resting-state networks. (A) Control group. The three seeds MO, dTh and Hip are in the same resting state network. (B) rTg4510 mice. The three seeds are in three different networks. Abbreviations: CPu - caudate-putamen, DCN - deep cerebellar nuclei, dTh - dorsal thalamus, GP - globus pallidus, Hip - hippocampus, MO - medial orbitofrontal cortex, pCtx - parietal cortex, S1 - primary somatosensory cortex, ST - stria terminalis.

Funding

This project was supported by DZNE (German Center for Neurodegenerative Diseases), MPG (Max Planck Society), Cure Alzheimer's Fund, and Katharina Hardt Foundation (to E.M. & E.M.M.).

Institutional support was received by DZNE, University Hospital Cologne and Forschungszentrum Jülich GmbH. The funding bodies did neither influence the design of the study, nor the collection, analysis, and interpretation of data or writing the manuscript.

CRediT authorship contribution statement

Heike Endepols: Conceptualization, Methodology, Investigation, Formal analysis, Writing – original draft. **Marta Anglada-Huguet:** Conceptualization, Methodology, Resources, Writing – review & editing. **Eckhard Mandelkow:** Conceptualization, Resources, Writing – review & editing, Funding acquisition. **Bernd Neumaier:** Conceptualization, Resources, Writing – review & editing. **Eva-Maria Mandelkow:** Conceptualization, Resources, Writing – review & editing, Funding acquisition. **Alexander Drzezga:** Conceptualization, Resources, Writing – review & editing.

Declaration of Competing Interest

The authors declare that they have no known competing financial interests or personal relationships that could have appeared to influence the work reported in this paper.

Data availability

Data will be made available on request.

Appendix A. Supplementary data

Supplementary data to this article can be found online at https://doi.org/10.1016/j.expneurol.2023.114632.

References

Andersen, K.B., Hansen, A.K., Knudsen, K., Schacht, A.C., Damholdt, M.F., Brooks, D.J., Borghammer, P., 2022. Healthy brain aging assessed with [^{18}F]FDG and [^{11}C]UCB-J PET. Nucl. Med. Biol. 112-113, 52–58.

Apetz, N., Kordys, E., Simon, M., Mang, B., Aswendt, M., Wiedermann, D., Neumaier, B., Drzezga, A., Timmermann, L., Endepols, H., 2019. Effects of subthalamic deep brain stimulation on striatal metabolic connectivity in a rat hemiparkinsonian model. Dis. Model. Mech. 12, dmm039065.

Ben-Nejma, I.R.H., Keliris, A.J., Daans, J., Ponsaerts, P., Verhoye, M., Van der Linden, A., Keliris, G.A., 2019. Increased soluble amyloid-beta causes early aberrant brain network hypersynchronisation in a mature-onset mouse model of amyloidosis. Acta Neuropathol. Commun. 7, 180.

Bero, A.W., Bauer, A.Q., Stewart, F.R., White, B.R., Cirrito, J.R., Raichle, M.E., Culver, J. P., Holtzman, D.M., 2012. Bidirectional relationship between functional connectivity and amyloid-beta deposition in mouse brain. J. Neurosci. 32, 4334–4340.

Chen, M.K., Mecca, A.P., Naganawa, M., Gallezot, J.D., Toyonaga, T., Mondal, J., Finnema, S.J., Lin, S.F., O'Dell, R.S., McDonald, J.W., Michalak, H.R., Vander Wyk, B., Nabulsi, N.B., Huang, Y., Arnsten, A.F., van Dyck, C.H., Carson, R.E., 2021. Comparison of [^{11}C]UCB-J and [^{18}F]FDG PET in Alzheimer's disease: a tracer kinetic modeling study. J. Cereb. Blood Flow Metab. 41, 2395–2409.

Coletta, L., Pagani, M., Whitesell, J.D., Harris, J.A., Bernhardt, B., Gozzi, A., 2020. Network structure of the mouse brain connectome with voxel resolution. Sci. Adv. 6, eabb7187.

Cui, D., Mesaros, A., Burdeos, G., Voigt, I., Giavalisco, P., Hinze, Y., Purrio, M., Neumaier, B., Drzezga, A., Obata, Y., Endepols, H., Xu, X., 2020. Dnmt3a2/Dnmt3L overexpression in the dopaminergic system of mice increases exercise behavior through signaling changes in the hypothalamus. Int. J. Mol. Sci. 21, 6297.

Degiorgis, L., Karatas, M., Sourty, M., Faivre, E., Lamy, J., Noblet, V., Bienert, T., Reisert, M., von Elverfeldt, D., Buee, L., Blum, D., Boutillier, A.L., Armspach, J.P., Blanc, F., Harsan, L.A., 2020. Brain network remodelling reflects tau-related pathology prior to memory deficits in thy-Tau22 mice. Brain 143, 3748–3762.

Delva, A., Michiels, L., Koole, M., Van Laere, K., Vandenberghe, W., 2022. Synaptic damage and its clinical correlates in people with early Huntington disease: a PET study. Neurology 98, e83–e94.

Di Re, J., Wadsworth, P.A., Laezza, F., 2017. Intracellular fibroblast growth factor 14: emerging risk factor for brain disorders. Front. Cell. Neurosci. 11, 103.

Dienel, G.A., Behar, K.L., Rothman, D.L., 2018. Cellular origin of [^{18}F]FDG-PET imaging signals during ceftriaxone-stimulated glutamate uptake: astrocytes and neurons. Neuroscientist 24, 316–328.

Drzezga, A., Becker, J.A., Van Dijk, K.R., Sreenivasan, A., Talukdar, T., Sullivan, C., Schultz, A.P., Sepulcre, J., Putcha, D., Greve, D., Johnson, K.A., Sperling, R.A., 2011. Neuronal dysfunction and disconnection of cortical hubs in non-demented subjects with elevated amyloid burden. Brain 134, 1635–1646.

Endepols, H., Anglada-Huguet, M., Mandelkow, E., Schmidt, Y., Krapf, P., Zlatopolskiy, B.D., Neumaier, B., Mandelkow, E.M., Drzezga, A., 2022. Assessment of the in vivo relationship between cerebral hypometabolism, tau deposition, TSPO expression, and synaptic density in a tauopathy mouse model: a multi-tracer PET study. Mol. Neurobiol. 59, 3402–3413.

Friston, K.J., 2011. Functional and effective connectivity: a review. Brain Connect. 1, 13–36.

Gamache, J., Benzow, K., Forster, C., Kemper, L., Hlynialuk, C., Furrow, E., Ashe, K.H., Koob, M.D., 2019. Factors other than hTau overexpression that contribute to tauopathy-like phenotype in rTg4510 mice. Nat. Commun. 10, 2479.

Goodwin, L.O., Splinter, E., Davis, T.L., Urban, R., He, H., Braun, R.E., Chesler, E.J., Kumar, V., van Min, M., Ndukum, J., Philip, V.M., Reinholdt, L.G., Svenson, K., White, J.K., Sasner, M., Lutz, C., Murray, S.A., 2019. Large-scale discovery of mouse transgenic integration sites reveals frequent structural variation and insertional mutagenesis. Genome Res. 29, 494–505.

Gopinath, K., Krishnamurthy, V., Cabanban, R., Crosson, B.A., 2015. Hubs of Anticorrelation in high-resolution resting-state functional connectivity network architecture. Brain Connect. 5, 267–275.

Grandjean, J., Canella, C., Anckaerts, C., Ayranci, G., Bougacha, S., Bienert, T., Buehlmann, D., Coletta, L., Gallino, D., Gass, N., Garin, C.M., Nadkarni, N.A., Hubner, N.S., Karatas, M., Komaki, Y., Kreitz, S., Mandino, F., Mechling, A.E., Sato, C., Sauer, K., Shah, D., Strobelt, S., Takata, N., Wank, I., Wu, T., Yahata, N., Yeow, L.Y., Yee, Y., Aoki, I., Chakravarty, M.M., Chang, W.T., Dhenain, M., von Elverfeldt, D., Harsan, L.A., Hess, A., Jiang, T., Keliris, G.A., Lerch, J.P., Meyer-Lindenberg, A., Okano, H., Rudin, M., Sartorius, A., Van der Linden, A., Verhoye, M., Weber-Fahr, W., Wenderoth, N., Zerbi, V., Gozzi, A., 2020. Common functional networks in the mouse brain revealed by multi-Centre resting-state fMRI analysis. Neuroimage 205, 116278.

Green, C., Sydow, A., Vogel, S., Anglada-Huguet, M., Wiedermann, D., Mandelkow, E., Mandelkow, E.M., Hoehn, M., 2019. Functional networks are impaired by elevated tau-protein but reversible in a regulatable Alzheimer's disease mouse model. Mol. Neurodegener. 14, 13.

Hall, G.R., Boehm-Sturm, P., Dirnagl, U., Finke, C., Foddis, M., Harms, C., Koch, S.P., Kuchling, J., Madan, C.R., Mueller, S., Sassi, C., Sotiropoulos, S.N., Trueman, R.C., Wallis, M.D., Yildirim, F., Farr, T.D., 2022. Long-term connectome analysis reveals reshaping of visual, spatial networks in a model with vascular dementia features. Stroke 53, 1735–1745.

Huo, B.B., Zheng, M.X., Hua, X.Y., Shen, J., Wu, J.J., Xu, J.G., 2021. Metabolic brain network analysis with 18F-FDG PET in a rat model of neuropathic pain. Front. Neurol. 12, 566119.

Jamadar, S.D., Ward, P.G.D., Liang, E.X., Orchard, E.R., Chen, Z., Egan, G.F., 2021. Metabolic and hemodynamic resting-state connectivity of the human brain: a high-temporal resolution simultaneous BOLD-fMRI and FDG-fPET multimodality study. Cereb. Cortex 31, 2855–2867.

Ji, M., Xia, J., Tang, X., Yang, J., 2018. Altered functional connectivity within the default mode network in two animal models with opposing episodic memories. PLoS One 13, e0202661.

Karatas, M., Noblet, V., Nasseef, M.T., Bienert, T., Reisert, M., Hennig, J., Yalcin, I., Kieffer, B.L., von Elverfeldt, D., Harsan, L.A., 2021. Mapping the living mouse brain neural architecture: strain-specific patterns of brain structural and functional connectivity. Brain Struct. Funct. 226, 647–669.

Kato, T., Inui, Y., Nakamura, A., Ito, K., 2016. Brain fluorodeoxyglucose (FDG) PET in dementia. Ageing Res. Rev. 30, 73–84.

Kordys, E., Apetz, N., Schneider, K., Duncan, E., Buschbell, B., Rohleder, C., Sue, M., Drzezga, A., Neumaier, B., Timmermann, L., Endepols, H., 2017. Motor impairment and compensation in a hemiparkinsonian rat model: correlation between dopamine depletion severity, cerebral metabolism and gait patterns. EJNMMI Res. 7, 68.

Laezza, F., Lampert, A., Kozel, M.A., Gerber, B.R., Rush, A.M., Nerbonne, J.M., Waxman, S.G., Dib-Hajj, S.D., Ornitz, D.M., 2009. FGF14 N-terminal splice variants differentially modulate Nav1.2 and Nav1.6-encoded sodium channels. Mol. Cell. Neurosci. 42, 90–101.

Liska, A., Galbusera, A., Schwarz, A.J., Gozzi, A., 2015. Functional connectivity hubs of the mouse brain. Neuroimage 115, 281–291.

Manno, F.A.M., Isla, A.G., Manno, S.H.C., Ahmed, I., Cheng, S.H., Barrios, F.A., Lau, C., 2019. Early stage alterations in white matter and decreased functional interhemispheric hippocampal connectivity in the 3xTg mouse model of Alzheimer's disease. Front. Aging Neurosci. 11, 39.

Marchitelli, R., Aiello, M., Cachia, A., Quarantelli, M., Cavaliere, C., Postiglione, A., Tedeschi, G., Montella, P., Milan, G., Salvatore, M., Salvatore, E., Baron, J.C., Pappata, S., 2018. Simultaneous resting-state FDG-PET/fMRI in Alzheimer disease: relationship between glucose metabolism and intrinsic activity. Neuroimage 176, 246–258.

Morrissey, Z.D., Gao, J., Zhan, L., Li, W., Fortel, I., Saido, T., Saito, T., Bakker, A., Mackin, S., Ajilore, O., Lazarov, O., Leow, A.D., 2022. Hippocampal functional connectivity across age in an app knock-in mouse model of Alzheimer's disease. Front. Aging Neurosci. 14, 1085989.

Passow, S., Specht, K., Adamsen, T.C., Biermann, M., Brekke, N., Craven, A.R., Ersland, L., Gruner, R., Kleven-Madsen, N., Kvernenes, O.H., Schwarzlmuller, T.,

Olesen, R.A., Hugdahl, K., 2015. Default-mode network functional connectivity is closely related to metabolic activity. Hum. Brain Mapp. 36, 2027–2038.
Pauwels, E.K., Ribeiro, M.J., Stoot, J.H., McCready, V.R., Bourguignon, M., Maziere, B., 1998. FDG accumulation and tumor biology. Nucl. Med. Biol. 25, 317–322.
Qi, J., Leahy, R.M., Cherry, S.R., Chatziioannou, A., Farquhar, T.H., 1998. High-resolution 3D Bayesian image reconstruction using the microPET small-animal scanner. Phys. Med. Biol. 43, 1001–1013.
Raichle, M.E., Mintun, M.A., 2006. Brain work and brain imaging. Annu. Rev. Neurosci. 29, 449–476.
Ramsden, M., Kotilinek, L., Forster, C., Paulson, J., McGowan, E., SantaCruz, K., Guimaraes, A., Yue, M., Lewis, J., Carlson, G., Hutton, M., Ashe, K.H., 2005. Age-dependent neurofibrillary tangle formation, neuron loss, and memory impairment in a mouse model of human tauopathy (P301L). J. Neurosci. 25, 10637–10647.
Riedl, V., Utz, L., Castrillon, G., Grimmer, T., Rauschecker, J.P., Ploner, M., Friston, K.J., Drzezga, A., Sorg, C., 2016. Metabolic connectivity mapping reveals effective connectivity in the resting human brain. Proc. Natl. Acad. Sci. U. S. A. 113, 428–433.
Rocher, A.B., Chapon, F., Blaizot, X., Baron, J.C., Chavoix, C., 2003. Resting-state brain glucose utilization as measured by PET is directly related to regional synaptophysin levels: a study in baboons. Neuroimage 20, 1894–1898.
Rohleder, C., Wiedermann, D., Neumaier, B., Drzezga, A., Timmermann, L., Graf, R., Leweke, F.M., Endepols, H., 2016. The functional networks of prepulse inhibition: neuronal connectivity analysis based on FDG-PET in awake and unrestrained rats. Front. Behav. Neurosci. 10, 148.
Sala, A., Lizarraga, A., Ripp, I., Cumming, P., Yakushev, I., 2022. Static versus functional PET: making sense of metabolic connectivity. Cereb. Cortex 32, 1125–1129.
Sala, A., Lizarraga, A., Caminiti, S.P., Calhoun, V.D., Eickhoff, S.B., Habeck, C., Jamadar, S.D., Perani, D., Pereira, J.B., Veronese, M., Yakushev, I., 2023. Brain connectomics: time for a molecular imaging perspective? Trends Cogn. Sci. 27, 353–366.
Santacruz, K., Lewis, J., Spires, T., Paulson, J., Kotilinek, L., Ingelsson, M., Guimaraes, A., DeTure, M., Ramsden, M., McGowan, E., Forster, C., Yue, M., Orne, J., Janus, C., Mariash, A., Kuskowski, M., Hyman, B., Hutton, M., Ashe, K.H., 2005. Tau suppression in a neurodegenerative mouse model improves memory function. Science 309, 476–481.
Schmitz, F., Silveira, J.S., Venturin, G.T., Greggio, S., Schu, G., Zimmer, E.R., Da Costa, J. C., Wyse, A.T.S., 2021. Evidence that methylphenidate treatment evokes anxiety-like behavior through glucose hypometabolism and disruption of the orbitofrontal cortex metabolic networks. Neurotox. Res. 39, 1830–1845.
Schwartz, W.J., Smith, C.B., Davidsen, L., Savaki, H., Sokoloff, L., Mata, M., Fink, D.J., Gainer, H., 1979. Metabolic mapping of functional activity in the hypothalamo-neurohypophysial system of the rat. Science 205, 723–725.
Shah, D., Jonckers, E., Praet, J., Vanhoutte, G., Delgado, Y.P.R., Bigot, C., D'Souza, D.V., Verhoye, M., Van der Linden, A., 2013. Resting state FMRI reveals diminished functional connectivity in a mouse model of amyloidosis. PLoS One 8, e84241.
Smith, S.M., Nichols, T.E., 2009. Threshold-free cluster enhancement: addressing problems of smoothing, threshold dependence and localisation in cluster inference. Neuroimage 44, 83–98.
Stafford, J.M., Jarrett, B.R., Miranda-Dominguez, O., Mills, B.D., Cain, N., Mihalas, S., Lahvis, G.P., Lattal, K.M., Mitchell, S.H., David, S.V., Fryer, J.D., Nigg, J.T., Fair, D. A., 2014. Large-scale topology and the default mode network in the mouse connectome. Proc. Natl. Acad. Sci. U. S. A. 111, 18745–18750.
TierSchG, 2006. Animal Welfare Act in the version published on May 18, 2006 (BGBl. I p. 1206, 1313), which was amended by Article 141 of the Act of March 29, 2017 (BGBl. I p. 626).
van Aalst, J., Ceccarini, J., Sunaert, S., Dupont, P., Koole, M., Van Laere, K., 2021. In vivo synaptic density relates to glucose metabolism at rest in healthy subjects, but is strongly modulated by regional differences. J. Cereb. Blood Flow Metab. 41, 1978–1987.
Wang, J., Xu, Y., Deshpande, G., Li, K., Sun, P., Liang, P., 2021. The effect of light sedation with midazolam on functional connectivity of the dorsal attention network. Brain Sci. 11, 1107.
Warnier, C., Lemaire, C., Becker, G., Zaragoza, G., Giacomelli, F., Aerts, J., Otabashi, M., Bahri, M.A., Mercier, J., Plenevaux, A., Luxen, A., 2016. Enabling efficient positron emission tomography (PET) imaging of synaptic vesicle glycoprotein 2A (SV2A) with a robust and one-step radiosynthesis of a highly potent ^{18}F-labeled ligand ([^{18}F]UCB-H). J. Med. Chem. 59, 8955–8966.
Whitesell, J.D., Liska, A., Coletta, L., Hirokawa, K.E., Bohn, P., Williford, A., Groblewski, P.A., Graddis, N., Kuan, L., Knox, J.E., Ho, A., Wakeman, W., Nicovich, P.R., Nguyen, T.N., van Velthoven, C.T.J., Garren, E., Fong, O., Naeemi, M., Henry, A.M., Dee, N., Smith, K.A., Levi, B., Feng, D., Ng, L., Tasic, B., Zeng, H., Mihalas, S., Gozzi, A., Harris, J.A., 2021. Regional, layer, and cell-type-specific connectivity of the mouse default mode network. Neuron 109 (545–559), e548.
Yakushev, I., Drzezga, A., Habeck, C., 2017. Metabolic connectivity: methods and applications. Curr. Opin. Neurol. 30, 677–685.
Zheng, A., Montez, D.F., Marek, S., Gilmore, A.W., Newbold, D.J., Laumann, T.O., Kay, B. P., Seider, N.A., Van, A.N., Hampton, J.M., Alexopoulos, D., Schlaggar, B.L., Sylvester, C.M., Greene, D.J., Shimony, J.S., Nelson, S.M., Wig, G.S., Gratton, C., McDermott, K.B., Raichle, M.E., Gordon, E.M., Dosenbach, N.U.F., 2021. Parallel hippocampal-parietal circuits for self- and goal-oriented processing. Proc. Natl. Acad. Sci. U. S. A. 118.